RATE AND COLLISION PROBABILITY OF TETHERS AND SAILS AGAINST DEBRIS OR SPACECRAFT

Ricardo García-Pelayo[†]*, Juan Luis Gonzalo*[⋆]*, Claudio Bombardelli*[†]

[†]Universidad Politécnica de Madrid
ETSIAE, Departamento de Física Aplicada
Plaza del Cardenal Cisneros, Madrid 28040, Spain
[⋆] Politecnico di Milano
Department of Aerospace Science and Technology
Via Giuseppe La Masa 34, Milan 20156, Italy

ABSTRACT

The work done on probability of collision between spherical objects in orbit is extended here to the case of one spherical object and one circular or rectangular object. The former is a model for spacecraft or debris, while the latter is a model for a sail or a tether. Two kinds of computations are done. The first kind is the computation of the collision rate when the flux of one object (typically debris) with respect to the other object is known. This information is important when planning a mission. The second kind is the computation of the collision probability for a particular pair of objects whose probability density functions of the positions are known. This information is necessary to decide if an evasive maneuver is going to be performed or not.

Index Terms— space debris; collision probability; collision rate; sail; tether;

1. INTRODUCTION

Estimating the rate or probability of collision between orbiting objects is a fundamental task in space security awareness. The rate is required, for instance, in order to assess the chance of a satellite experiencing one or more collisions in its lifetime as it interacts with the surrounding debris environment. The probability of collision needs to be computed whenever an active spacecraft experiences a critical conjunction in order to determine whether or not a propulsive collision avoidance maneuver should be performed. Lastly, if a maneuver is eventually required it can only be optimized with the aid of a proper collision probability estimation method [1].

There is an abundant literature dealing with the computation of the collision probability when the two approaching bodies are spheres [2, 3, 4, 5, 6, 7]. Of these, the methods [6, 7] are the most computationally efficient. Method [7] is the only one that can be applied to the non-Gaussian case.

The spherical envelope of the true spacecraft geometry provides a good conservative bound of the collision probability for the case of, say, two satellites. But it becomes overly simplistic when at least one of the two objects is far from spherical. Large circular or rectangular solar sails of tens to hundreds of square meters surface and km-long tethers, for instance, are envisioned as passive deorbiting devices to be deployed at the end-of-life of future spacecraft to provide a low-cost reentry in low earth orbit (LEO). Actually the European Space Agency is interested in the computation of the rate and probability of collision that we mentioned in the first paragraph. This is part of the study in which the authors have been involved and which has motivated them to write the present paper.

The need to compute collision probabilities and rates of non spherical objects has been recognized before. An outline of how to decompose the International Space Station into rectangular pieces to compute its probability of collision is given in Chapter 6 of [4]. More recently a computation of the collision probability for rectangular cross section was presented [8], but it used some approximations that we do without in the present article.

There is a software [9] which can be used to compute the rate of collision of orbiting ellipsoids, and an ellipsoid can be a sphere and can be made to approach a tether. But this approach works with pairs of satellites and requires a catalog, whereas our approach is analytical and we work with a satellite and a flux obtained from a database (for example ORDEM [10] or MASTER [11]).

The attitude of a dead satellite is a complicated matter, but taking its attitude to be random is a reasonable assumption ([12], p. 13). Taking the maximum projected area on the collision plane seems to be a conservative assumption, and this has been done for cuboids [13, 14] and therefore for rectangles as a particular case. But if an upper bound of the actual projection area is used, the deorbiting time is underestimated, therefore it is not clear if taking the maximum projected area is actually a safer option than taking the attitude to be random.

The goal of this article is to provide formulae for the collision rate and the collision probability of tethers and rectangular or circular sails (henceforth, body MM) against satellites or debris, modeled by spheres (henceforth, body SS). All of the results are analytical except for the calculation of the collision probability of a rectangle and a sphere, for which a very efficient program has been written.

In section 2 the general theoretical setup of this article is laid down. In section 3 we are interested in the rate of collision of body MM with *any* satellite or debris over a long interval of time. A typical use of this rate is to estimate the survival probability of a certain mission. In subsection 3.1 the projection M of MM onto the encounter plane stays the same over the long interval of time. In subsection 3.2 MM tumbles around randomly. In section 4 the probability of collision of body MM against one particular body SS is found. We suppose that the conditions of short-encounter model [2, 15, 3, 5, 4, 16, 1, 6] are fulfilled and that the probability density functions (henceforth, pdf) of the positions of both body MM and body SS are known. A typical use of this probability of collision is to decide if an evasive maneuver is going to be made or not. In section 5 some conclusions are stated.

2. PROBABILITY OF COLLISION DURING A SHORT ENCOUNTER

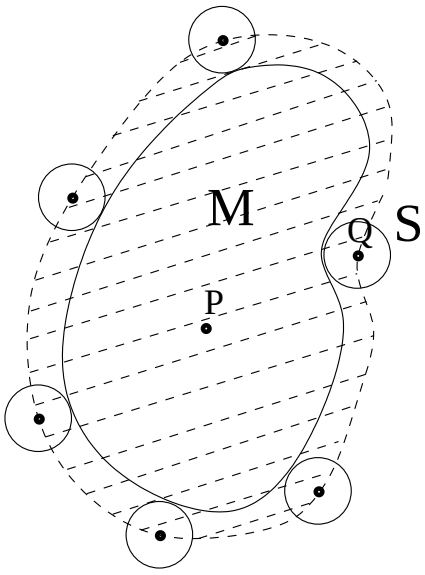

Fig. 1. The collision region in the encounter plane is found by sliding the projection of the debris or the satellite (the circle S) around the projection M.

Whether we want to find collision rate or the collision probability, the first step is to find the region of collision in the encounter plane, which is the plane perpendicular to the relative velocity $\vec{v}$ of bodies MM and SS. Let M and S denote the projections of bodies MM and SS onto the encounter plane (also known as b-plane). Then, as shown in Fig. 1, the collision region is the shaded region, which is obtained by sliding S (the projection of the debris or the satellite) around M. When the S comes back to its original position, the point Q shown in Fig. 1 has drawn the contour of the shaded region. We shall denote the shaded region by $M \oplus (-S)$, because it is the Minkowski sum of the projections of M and the inversion of S ([17], remark at the end of p. 12).

For a more complicated example of Minkowski sum of two projections of spacecraft, see Fig. 11 of [18].

Let ρ be the pdf of the vector $\overrightarrow{PQ}$ (see Fig. 1). Then the probability of collision between MM and SS is

$$\int_{M \oplus (-S)} d^2 r \; \rho(\vec{r}). \tag{1}$$

In order to find the collision probability we need both the dashed region Ms and ρ. But to find the rate the latter will suffice.

We now show how to find the projection ρ of the pdf of the relative position $\overrightarrow{PQ}$ onto the encounter plane.

We assume that pdf's of the positions P and Q, ρ_P and ρ_Q, respectively, are given. That is, $\rho_P(\vec{r}) \; d^3 r$ is the probability that the point P is in the interval $[x, x+dx] \times [y, y+dy] \times [z, z+dz]$, and a similar statement defines ρ_Q. Then, since ρ_P and ρ_Q are independent, the probability density that $\overrightarrow{PQ}$ be equal to $\vec{r}$ is the integral over all possible ways in which the positions of P and Q differ by a vector $\vec{r}$, that is,

$$\begin{aligned} \rho_{rel}(\vec{r}) &= \int d^3 r' \; \rho_P(\vec{r}') \rho_Q(\vec{r} + \vec{r}') = \\ &= \int d^3 r' \; \rho_P(-\vec{r} + \vec{r}') \rho_Q(\vec{r}'). \end{aligned} \tag{2}$$

Note that if ρ_P and ρ_Q are Gaussians, then ρ_{rel} is also a Gaussian.

ρ is the projection of ρ_{rel} onto the encounter plane, that is for any $\vec{r}$ in the encounter plane,

$$\rho(\vec{r}) = \int d\lambda \; \rho_{rel}(\vec{r} + \lambda \vec{v}), \tag{3}$$

where $\vec{v}$ is the relative velocity. Note that ρ is a marginal distribution.

3. RATE OF COLLISION OVER A LONG INTERVAL OF TIME

In the present section we provide a general scheme to assess the collision probability of a non-spherical body MM with a population of spherical debris over an interval of time which includes many orbital periods.

Strictly speaking, collisions are correlated random events. For example, debris originated in an explosion appears in clouds [19], so that if a collision with a piece of debris in the cloud has taken place, then for a short period of time the satellite is likely to still be in that cloud and has a larger than usual probability of colliding again. Debris of astronomical origin which is in solar orbit also comes in clouds. However, collisions are very unlikely, and the mean time between collisions is much larger than the time that the satellite spends in a cloud. Therefore, over long intervals of time, collisions are uncorrelated random events. Therefore their occurrence is a Poisson process [20] whose rate we want to determine. It follows from (1) that, on the average, the probability that the result of flyby is a collision is

$$\bar{\rho}\ \mathrm{A}(M \oplus S), \tag{4}$$

where $\mathrm{A}(M \oplus S)$ is the area of the Minkowski sum and $\bar{\rho}$ is the average value of ρ. In a flyby $\bar{\rho}$ is the inverse of the area of the region of the encounter plane where the incoming debris might be found. The rate of collision of the Poisson process is $\bar{\rho}\mathrm{A}(M \oplus S)$ divided by the time Δt between flybys. We now determine this rate.

For each incoming sphere SS there is a different encounter plane which yields a different Minkowski sum $M \oplus S$. We are going to derive first the case in which all of the incoming spheres have the same size and direction. Let ϕ be their flux in the MM system of reference. For example this flux can be obtained from the ORDEM [10] or MASTER [11] databases, where it is given in the system of reference of an object MM whose orbital parameters are given by the user. These spheres SS are normally incident on $M \oplus S$. $\bar{\rho}$ is a surface density of spheres SS, because it has dimensions of L^{-2} (inverse length squared). The number of spheres SS incident on $M \oplus S$ during a time Δt is, by definition of flux, equal to $\phi A(M \oplus S)\Delta t$. The surface density of spheres on $M \oplus S$ is then $\phi \Delta t = \bar{\rho}$ and the Poisson rate wanted in the last sentence of the last paragraph is $\phi A(M \oplus S)$. The probability of n collisions during an interval t is

$$e^{-\phi \mathrm{A}(M \oplus S)t}\ \frac{(\phi \mathrm{A}(M \oplus S))^n}{n!}. \tag{5}$$

The most interesting case is $n = 0$, which yields the survival probability, $e^{-\phi \mathrm{A}(M \oplus S)t}$.

Note that eq. (5) is a generalization of formula (3.2) in [21]. Indeed, formula (3.2) in [21] is formula (5) with $\mathrm{A}(M \oplus S))$ substituted by $\mathrm{A}(M)$. When the size of the debris is small compared to the size of MM, formula (3.2) in [21] may be used. When SS is large debris or satellites, their size must be included in the analysis and expression (5) must be used.

So far we have obtained the collision rate for fixed size and incoming direction of the spheres SS. For an arbitrary distribution of sizes and incoming directions one has to weigh by the distribution and integrate over the sizes of the spheres and the directions of the flux.

3.1. Fixed attitude with respect to the encounter plane

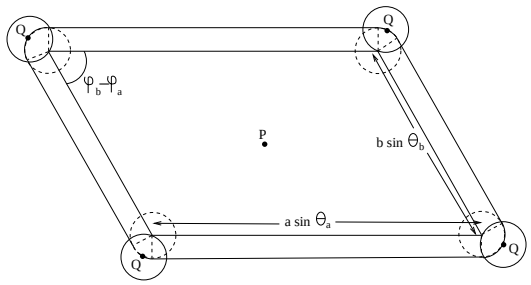

Fig. 2. Minkowski sum of a rectangle and a sphere.

Most of the time, collision is with small debris. Then the rim in Fig. 1 is negligible and $\mathrm{A}(M \oplus S)$ may be very well approximated by $\mathrm{A}(M)$. However, tethers and sails may also collide with active or dead spacecraft, whose sizes are not negligible compared to the size of the sail or tether. Then the area of the rim in Fig. 1 (that is, the region between M and $M \oplus (-S)$) has to be taken into account. When the projection M is a parallelogram and the radius of the sphere is R, it is clear from Fig. 2 that the area of $M \oplus S$ is the projected area of the rectangle + (the projected perimeter of the rectangle $\times$ R) + πR^2, that is

$$\mathrm{A}(M \oplus S) = \mathrm{A}(M) + \mathrm{per}(M)R + \pi R^2, \tag{6}$$

where $\mathrm{per}(M)$ is the perimeter of M. This formula holds whenever the projection M is convex. Indeed, the Steiner-Minkowski theorem gives a formula for the computation of the n-dimensional volume of Minkowski sums of convex bodies and spheres. When $n = 2$ this formula is simply the above formula ([22], p. 116).

In this section we are going to find the area $\mathrm{A}(M \oplus S)$ to be substituted in formula (5) for a rectangular sail, a tether and a circular sail.

3.1.1. Rectangle

The projection of a rectangle onto a plane is a parallelogram. Indeed, a projection is a linear transformation (see, e. g., [23], p. 113). Therefore, it transforms parallel lines into parallel lines.

Fig. 2 is useful to follow parts of this paragraph. Let θ_a and θ_b be the angles made by the direction of the relative velocity and the directions of the sides of the rectangular sail (see Fig. 3). We define a Cartesian coordinate frame whose z-axis is parallel to $\vec{v}$. Then we define spherical coordinates where θ is the colatitude (angle made with the positive direction of the z-axis) and φ is the longitude. The coordinates of the unit vectors associated with the sides of the sail are $\vec{u}_a = (\sin\theta_a \cos\varphi_a, \sin\theta_a \sin\varphi_a, \cos\theta_a)$ and $\vec{u}_b = (\sin\theta_b \cos\varphi_b, \sin\theta_b \sin\varphi_b, \cos\theta_b)$. The cosine of the angle

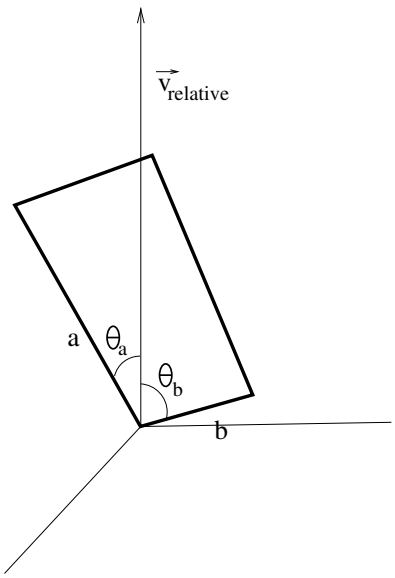

Fig. 3. Angles θ_a and θ_b are shown.

θ_M made by the z-axis and the vector perpendicular to the sail is the third component of $\vec{u}_a \times \vec{u}_b$, which is

$$\cos\theta_M = \sin(\varphi_b - \varphi_a)\sin\theta_a \sin\theta_b. \tag{7}$$

Since $\vec{u}_a$ and $\vec{u}_b$ are perpendicular, $\vec{u}_a \cdot \vec{u}_b = \cos\theta_a\cos\theta_b + \sin\theta_a\sin\theta_b\cos(\varphi_b - \varphi_a) = 0 \Rightarrow$

$$\cos(\varphi_b - \varphi_a) = -\frac{\cos\theta_a\cos\theta_b}{\sin\theta_a\sin\theta_b}. \tag{8}$$

Therefore,

$$\begin{aligned} A(M) &= ab\cos\theta_M = \\ &= ab\sqrt{1 - \left(\frac{\cos\theta_a\cos\theta_b}{\sin\theta_a\sin\theta_b}\right)^2}\sin\theta_a\sin\theta_b = \\ &= ab\sqrt{-\cos(\theta_a+\theta_b)\cos(\theta_a-\theta_b)} \end{aligned} \tag{9}$$

and

$$\begin{aligned} \mathrm{A}(M \oplus (-S)) = ab\sqrt{-\cos(\theta_a+\theta_b)\cos(\theta_a-\theta_b)} + \\ 2(a\sin\theta_a + b\sin\theta_b)R + \pi R^2. \end{aligned} \tag{10}$$

This is the expression to be substituted in equation (5).

Of course $M \oplus (-S)$ in Fig. 2 could have been circumscribed by a larger parallelogram, but the formula for its area is not simpler than the preceding exact formula.

3.1.2. Tether

We have seen that the projection of a rectangle is not a rectangle but (in general) a parallelogram. Likewise, the projection of a cylindrical or tape tether onto a plane is not a rectangle.

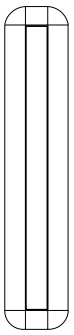

Fig. 4. Minkowski sum of a rectangle and a disk. Only the two large contributions at the sides are kept in expression (11).

However, the difference between its projection and a rectangle is very small. This is because the length to width ratio of tethers is of the order of 10^5. Furthermore, a subsatellite of non negligible size and mass is in most of the cases attached to the tether end for various purposes. For instance in a mechanical tether it can be a ballast mass to ease the tether deployment, while in an electrodynamic tether the subsatellite may host an electron emitting device (e.g. a hollow cathode) to maximize the transmitted current. Therefore we may forget about the non-rectangular part of the projection altogether.

We denote α to be the angle made by the tether and the collision plane.

Case 1) Round tether of radius r and length L. Its projection on the collision plane is a rectangle of width $2r$ and length $L\cos\alpha$. According to the formula (6), $\mathrm{A}(M \oplus S) = 2rL\cos\alpha + 2R(2r + L\cos\alpha) + \pi R^2$. However, as explained at the beginning of this subsubsection, we neglect the contributions of the ends of the tether, because that part of the Minkowski sum is going to be taken into account by the Minkowski sum of the satellite or the hollow cathode and the sphere. Therefore we just keep the contribution (see Fig. 4)

$$2rL\cos\alpha + 2RL\cos\alpha = 2(R+r)L\cos\alpha. \tag{11}$$

If the sphere is not small debris but a satellite, the above expression may be approximated by $2RL\cos\alpha$.

Case 2) The tether is a tape of length L, width w (a typical value for w would be 2 cm) and negligible thickness. The edges of the tape are not straight; the tape is twisted and its projection on a plane has sinusoidal edges, as shown in Fig. 5. While a computation of the Minkowski sum is in principle possible, one may also substitute the actual projection by a rectangle with the same axis of symmetry and width $2w/\pi$, which has the same area as the actual projection (see Fig. 5). Indeed, let β be the angle made by some straight line and some segment. We compute the average of the projection of the segment over the straight line over the range $[0, \pi/2]$, which, by symmetry, is the same as the average over the range $[0, 2\pi]$. The probability density function of the uniform den-

sity in the range $[0, \pi/2]$ is the constant $\frac{1}{\pi/2}$. Therefore the factor by which the length of the segment has to be multiplied is $\int_0^{\pi/2} d\beta \, \frac{\cos\beta}{\pi/2} = \frac{2}{\pi}$. Thus if w is the width of the tape, $2w/\pi$ is its twisted width. With this approximation, the projection on the collision plane is a rectangle of width $2w/\pi$ and length $L\cos\alpha$. According to formula (6), the area of the Minkowski sum is $((2w/\pi)L\cos\alpha + 2R((2w/\pi + L\cos\alpha)) + \pi R^2$. For the same reasons that lead to expression (11), we just keep the contribution

$$\frac{2w}{\pi} L\cos\alpha + 2RL\cos\alpha = 2\Big(\frac{w}{\pi} + R\Big) L\cos\alpha. \qquad (12)$$

If the sphere is not small debris but a satellite, the above expression may be approximated by $2RL\cos\alpha$.

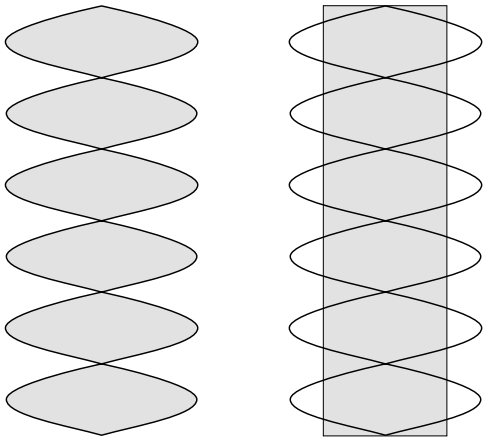

Fig. 5. To the left, projection of a twisted tape on to a plane. To the right, projection of a twisted tape on to a plane and a rectangle of the same area.

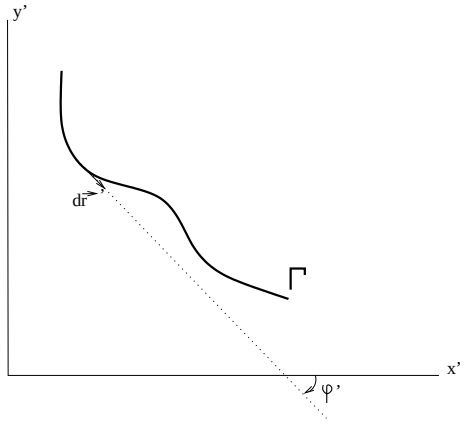

Fig. 6. Curve Γ to be projected onto the xy plane.

3.1.3. Disk

First we show that the projection of a disk of radius a onto a plane pl is an ellipse. Let θ_M be the angle between pl and the plane which contains the disk. Construct a Cartesian coordinate frame whose x-axis is the intersection between the plane which contains the disk and the plane pl, whose z-axis is perpendicular to the plane pl and whose y-axis is perpendicular to the other two and completes a right-handed frame. Then the projection of the diameter of the disk which is parallel to the x-axis still has radius a, but all chords perpendicular to the said diameter shrink by a factor $\cos\theta_M$ when projected. An ellipse of semiaxes a and b can be obtained from a disk of radius a by a dilation, as is clear from the Cartesian formula $(x/a)^2 + (y/b)^2 = 1$. Therefore the said projection is indeed an ellipse of semiaxes a and $a\cos\theta_M$.

The perimeter of an ellipse of semiaxes a and b is $4aE\Big(1 - \frac{b^2}{a^2}\Big)$, where E is the complete elliptic integral of the second kind. It follows that

$$\mathrm{A}(M \oplus S) = \pi R_{sail}^2 \cos\theta_M + 4R_{sail} E(\sin^2\theta_M) R + \pi R^2, \qquad (13)$$

where R_{sail} is the radius of the disk. This is the expression to be substituted in equation (5).

3.2. Random attitude

If we take the attitude of body MM to be random, then we need to compute the average area of $M \oplus S$ when the attitude of body MM is averaged over. Fortunately, as we shall see, there is a simple formula when MM is a flat, convex surface.

Lemma. Let ℓ be the length of a flat curve Γ (i. e., $\int_\Gamma dr = \ell$) contained in a plane whose normal makes an angle θ with the z-axis. Then the average (with respect to rotations of the curve Γ in its plane) of the length of the projection of the curve Γ onto the xy-plane is

$$\frac{2}{\pi} E(\sin^2\theta)\ell, \qquad (14)$$

where E is the complete elliptic integral of the second kind.

Proof. Let x' and y' be Cartesian coordinates for the plane in which the curve Γ lies. We may, without loss of generality, suppose that the axis x' and the axis x are the same, so that the normal to the plane containing the curve Γ is contained in the yz-plane. Consider an oriented element of length $d\vec{r}'$ of the curve Γ which makes an angle φ' with the x'-axis, that is, $d\vec{r} = |d\vec{r}|(\cos\varphi', \sin\varphi', 0)$. In x, y, z coordinates the unit vector $(\cos\varphi', \sin\varphi', 0)$ is

$$\begin{pmatrix} 1 & 0 & 0 \\ 0 & \cos\theta & \sin\theta \\ 0 & -\sin\theta & \cos\theta \end{pmatrix} \begin{pmatrix} \cos\varphi' \\ \sin\varphi' \\ 0 \end{pmatrix} = \begin{pmatrix} \cos\varphi' \\ \sin\varphi'\cos\theta \\ -\sin\varphi'\sin\theta \end{pmatrix}. \qquad (15)$$

The length of the projection of the unit vector on the xy-plane is $\sqrt{\cos^2\varphi' + \sin^2\varphi'\cos^2\theta}$. The average of this expression

over the angle φ' is

$$\frac{2}{\pi}\int_0^{\frac{\pi}{2}} d\varphi' \sqrt{\cos^2\varphi' + \sin^2\varphi'\cos^2\theta} = \frac{2}{\pi}E(\sin^2\theta). \quad (16)$$

Therefore the average projected length is

$$\frac{2}{\pi}\int_0^{\frac{\pi}{2}} d\varphi' \int_\Gamma dr \sqrt{\cos^2\varphi' + \sin^2\varphi'\cos^2\theta} = \int_\Gamma dr\, \frac{2}{\pi}E(\sin^2\theta) = \frac{2}{\pi}E(\sin^2\theta)\ell. \quad \textbf{QED}. \quad (17)$$

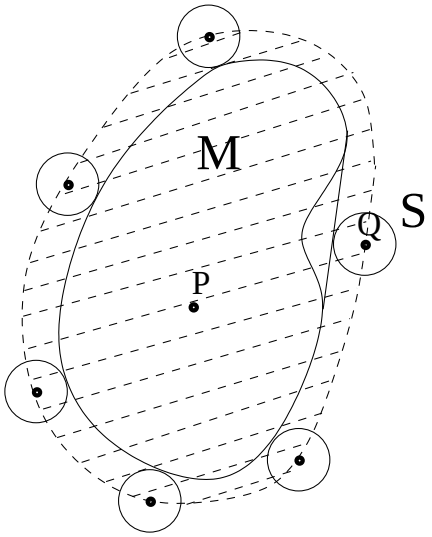

Fig. 7. It is seen in this example that $M \oplus S \subset M_{env} \oplus S$, as proven in the text.

Note that the above lemma is true regardless of whether the curve Γ is open or closed, convex or concave. The formula for the length of an ellipse, $4aE\left(1-\frac{b^2}{a^2}\right)$, is a particular case of the above formula, since an ellipse of semiaxes a and b is the projection on the xy-plane of a circle which makes an angle $\arccos(b/a)$ with the said plane.

The projected surface of a flat figure of area A contained in a plane whose normal makes an angle θ with the z-axis is $A\cos\theta$. The element of surface in spherical coordinates is $r^2\sin\theta\, d\theta\, dr$. Therefore, the probability that the colatitude be θ is proportional to $\sin\theta$. Since $\int_0^{\pi/2} d\theta\ \sin\theta = 1$, the Steiner-Minkowski formula (6) yields that the average collision cross section when the orientation of a convex flat figure is isotropic is

$$\int_0^{\pi/2} d\theta \sin\theta\left(A\cos\theta + \frac{2}{\pi}E(\sin^2\theta)\ell R + \pi R^2\right) = \frac{A}{2} + \frac{\pi\ell R}{4} + \pi R^2. \quad (18)$$

Example 1. The figure is a **rectangle** of sides a and b. Its average collision cross section is

$$\overline{\mathrm{A}(M\oplus S)} = \frac{ab}{2} + \frac{\pi(a+b)R}{2} + \pi R^2. \quad (19)$$

Example 2. The figure is a **disk** of radius R_{sail}. Its average collision cross section is

$$\overline{\mathrm{A}(M\oplus S)} = \frac{\pi R_{sail}^2}{2} + \frac{\pi^2 R_{sail}R}{2} + \pi R^2. \quad (20)$$

For the reasons given in subsubsection 3.1.2, the case of the tether ($b << a$) would be $\frac{ab}{2} + \frac{\pi aR}{2}$, with b the width of the cylindrical tether, or $b = 2/\pi$ times its width if it is a tape. However, the attitude of the tether is not random, because of the large disparity between its moments of inertia and the gravity gradient [24].

The convex envelope of a body is the smallest convex body which contains it. When this body is a flat figure, the convex envelope is the figure made by a rubber band which surrounds the figure. It is intuitive that, as depicted in Fig. 7, $M \oplus S \subset M_{env} \oplus S$. Indeed, $M \subset M_{env} \Rightarrow M_{env} = M \cup M'$, where $M' = M_{env} - M$. The Minkowski sum is distributive with respect to the union of sets, therefore $M_{env} \oplus S = (M \oplus S) \cup (M' \oplus S) \supset M \oplus S$.

We use this result to bound the average collision cross section of a **concave** flat figure:

$$\overline{\mathrm{A}(M\oplus S)} \leq \frac{A_{env}}{2} + \frac{\pi\ell_{env}R}{4} + \pi R^2, \quad (21)$$

where A_{env} and ℓ_{env} are the area and the perimeter of the convex envelope, respectively.

4. PROBABILITY OF COLLISION FOR RECTANGLES, TETHERS AND DISKS

We are going to suppose that ρ_{rel} is a Gaussian, because the pdf's of the position, in terms of which ρ_{rel} is defined, are almost always given as Gaussians. Then the integral in (1) cannot be done for arbitrary Ms. In particular, it cannot be done for the Minkowski sum of a circle and an ellipse or the Minkowski sum of a circle and a parallelogram. However, the Minkowski sum of a circle and an ellipse, and the Minkowski sum of a circle and a parallelogram can be tightly enclosed by an ellipse and by a parallelogram, respectively. Good analytical approximations for the computation of the integral in (1) are available when Ms is the ellipse or the parallelogram, as we shall see.

4.1. The rectangle

An upper bound for the probability of collision is

$$\int_{Par(Ms)} \rho(\vec{r}), \quad (22)$$

where $Par(Ms)$ is the enclosing parallelogram shown in Fig. 8 of the Minkowski sum shown in Fig. 2. If R is the radius of the sphere, the sides of the enclosing parallelogram are at a distance R from the projection of the rectangle. We need to find the length added to each of the sides shown in Figure 8. In the left figure the two kinds of kites whose sides we need to find are shown in dashed lines. The angles made by the sides of the kites which join at the vertex of the parallelogram are $\varphi_b - \varphi_a$ for the right upper kite and $\pi - (\varphi_b - \varphi_a)$ for the right lower kite. In the right figure, the angle made by the two segments of length R is $\pi - (\varphi_b - \varphi_a)$. It is easy to see that the length of the dotted segment is $2R\sin((\pi - (\varphi_b - \varphi_a))/2) = 2R\cos((\varphi_b - \varphi_a)/2)$. The larger triangle is an isosceles triangle whose angles have values $(\pi - (\varphi_b - \varphi_a))/2$ and $\varphi_b - \varphi_a$. It follows from the sine theorem that $x = 2R\cos^2((\varphi_b - \varphi_a)/2)/\sin(\varphi_b - \varphi_a) = R\tan\frac{\pi-(\varphi_b-\varphi_a)}{2}$. Likewise, for the right upper kite the added length is $x = 2R\sin^2((\varphi_b - \varphi_a)/2)/\sin(\varphi_b - \varphi_a) = R\tan\frac{\varphi_b-\varphi_a}{2}$. Then the length added to each of the sides is

$$\begin{aligned} &R\tan\frac{\pi-(\varphi_b-\varphi_a)}{2} + R\tan\frac{\varphi_b-\varphi_a}{2} = \\ &= \frac{2R}{\sin(\varphi_b-\varphi_a)} = \frac{R\sin(\theta_a+\theta_b)}{\sqrt{-\cos(\theta_a+\theta_b)\cos(\theta_a-\theta_b)}}, \end{aligned} \tag{23}$$

where the last equality can be obtained from eqs. (8) and (9).

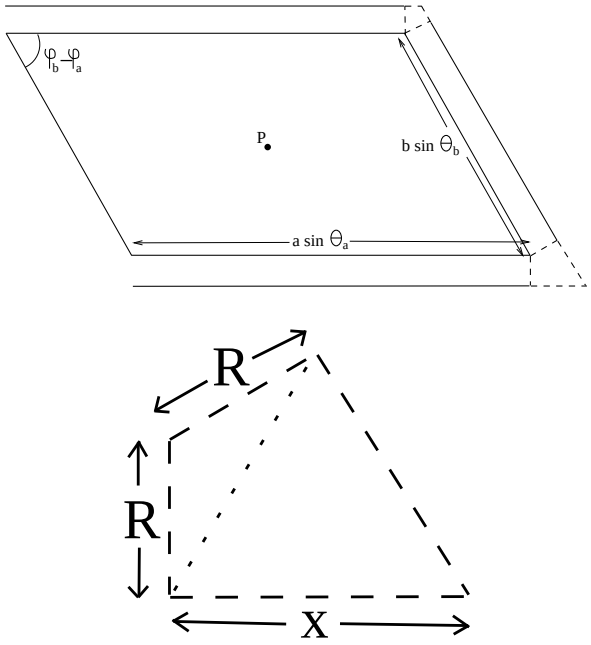

Fig. 8. In the top figure the two kinds of kites whose sides we need to find are shown in dashed lines. In the bottom figure one of them is amplified.

The enclosing parallelogram is now completely determined. The problem at hand is to evaluate the integral

$$\frac{1}{2\pi\sigma_x\sigma_y}\int_{Par(Ms)} d^2r\ \exp -\frac{1}{2}\left(\frac{x^2}{\sigma_x^2}+\frac{y^2}{\sigma_y^2}\right), \tag{24}$$

which is a tight upper bound for the collision probability. In order to do this integral we shall develop a method for the computation of bivariate normal probabilities in rectangular domains based on the work of Genz [25].

In [25] Genz proposes and compares several algorithms for the numerical computation of bivariate, trivariate normal distribution and Student t probability distributions. In particular, a very fast algorithm is presented for computing the bivariate normal probability $L(h,k,\rho)$ for a domain of the form $[h,\infty)\times[k,\infty)$ $(h,k\in\Re)$ and a Gaussian of correlation $\rho\in[0,1]$ and $\sigma_x = \sigma_y = 1$. Note that L is related to the standard bivariate normal cumulative distribution Φ by the expression $\Phi((x,y),\rho) = L(-x,-y,\rho)$.

To apply this algorithm, the domain and the covariance matrix have to be transformed so that the former becomes a rectangle and the latter a correlation matrix. Let $V_0 = (x_0, y_0)$ be a vertex of the parallelogram, and let $(x_1,y_1),(x_2,y_2)$ be the coordinates of the two vertices adjacent to V_0. We define

$$\begin{aligned} \vec{a} &= (a_x, a_y) \equiv (x_1,y_1) - (x_0,y_0), \\ \vec{b} &= (b_x, b_y) \equiv (x_2,y_2) - (x_0,y_0), \end{aligned} \tag{25}$$

where $\vec{a}$ and $\vec{b}$ are the vectors representing the sides of the parallelogram departing from V_0. It is then possible to find a linear transformation, defined by matrix M, that transforms the parallelogram into a square of unit side by imposing:

$$M\vec{a} = \begin{pmatrix} 1 \\ 0 \end{pmatrix}, \quad M\vec{b} = \begin{pmatrix} 0 \\ 1 \end{pmatrix}. \tag{26}$$

Combining these two equations and solving for M yields:

$$M \equiv \begin{pmatrix} a_x & b_x \\ a_y & b_y \end{pmatrix}^{-1} \tag{27}$$

Note that the resulting linear transformation will exist as long the matrix formed by $\vec{a}$ and $\vec{b}$ is invertible, that is, if both vectors are linearly independent. This condition will be met by any non-degenerate parallelogram.

The new domain is a square of unit side, defined by vertex

$$V_0^* = \begin{pmatrix} x_0^* \\ y_0^* \end{pmatrix} \equiv MV_0\,, \tag{28}$$

and side vectors $\vec{a}^* = (a_x^*, a_y^*) \equiv (1,0)$ and $\vec{b}^* = (b_x^*.b_y^*) \equiv (0,1)$. The covariance matrix will transform to:

$$\begin{pmatrix} \sigma_x^{*2} & \sigma_{xy}^* \\ \sigma_{xy}^* & \sigma_y^{*2} \end{pmatrix} \equiv M \begin{pmatrix} \sigma_x^2 & 0 \\ 0 & \sigma_y^2 \end{pmatrix} M^T, \tag{29}$$

which is in general not diagonal.

In the algorithm by Genz a correlation matrix instead of a covariance matrix is used, so one final transformation is needed. By applying two dilations (or contractions) of magnitudes $1/\sigma_x^*$ and $1/\sigma_y^*$ along the x and y axes, respectively, the covariance matrix becomes a correlation matrix:

$$\begin{pmatrix} 1 & \rho' \\ \rho' & 1 \end{pmatrix} \equiv \begin{pmatrix} 1 & \sigma_{xy}^*/\sigma_x^*\sigma_y^* \\ \sigma_{xy}^*/\sigma_x^*\sigma_y^* & 1 \end{pmatrix}, \tag{30}$$

and the domain becomes a rectangle of vertex

$$V_0' = \begin{pmatrix} x_0' \\ y_0' \end{pmatrix} \equiv \begin{pmatrix} x_0^*/\sigma_x^* \\ y_0^*/\sigma_y^* \end{pmatrix}, \tag{31}$$

and side vectors $\vec{a}' = (a_x', a_y') \equiv (1/\sigma_x^*, 0)$ and $\vec{b}' = (b_x', b_y') \equiv (0, 1/\sigma_y^*)$.

Calling $Rect$ the new domain, it is possible to write

$$\begin{gathered} \frac{1}{2\pi\sigma_x\sigma_y}\int_{Par(Ms)} d^2r \exp -\frac{1}{2}\left(\frac{x^2}{\sigma_x^2}+\frac{y^2}{\sigma_y^2}\right) = \\ \frac{1}{2\pi\sqrt{1-\rho'^2}}\int_{Rect} d^2r \exp \frac{-(x^2-2\rho' xy-y^2)}{2(1-\rho'^2)} = \\ \Phi(Rect,\rho'), \end{gathered} \tag{32}$$

where the latter can be computed numerically by combining four calls to the bivariate normal probability function considered by Genz:

$$\begin{gathered} \Phi(Rect,\rho') = L(x_0',y_0',\rho') - L(x_0'+a_x',y_0',\rho') - \\ L(x_0',y_0'+b_y',\rho') + L(x_0'+a_x',y_0'+b_y',\rho'). \end{gathered} \tag{33}$$

We have programmed a web app implementing $\Phi(Rect,\rho')$ in JavaScript, which can be found at `http://sdg.aero.upm.es/index.php/online-apps/gaussian-over-parallelogram`.

4.2. The very thin rectangle (tether)

If the body MM is a tether then we can approximate its projection on the encounter plane by a rectangle, as argued in subsubsection 3.1.2.

The probability caught by a rectangle of axes parallel to the principal axes of a Gaussian is

$$\begin{gathered} \int_{x_1}^{x_2} dx\, \frac{e^{-\frac{1}{2}\frac{x^2}{\sigma_x^2}}}{\sqrt{2\pi\sigma_x^2}} \int_{y_1}^{y_2} dy\, \frac{e^{-\frac{1}{2}\frac{y^2}{\sigma_y^2}}}{\sqrt{2\pi\sigma_y^2}} = \\ \frac{1}{2}\left(\operatorname{erf}\Big(\frac{x_2}{\sqrt{2}\sigma_x}\Big) - \operatorname{erf}\Big(\frac{x_1}{\sqrt{2}\sigma_x}\Big)\right) \cdot \\ \frac{1}{2}\left(\operatorname{erf}\Big(\frac{y_2}{\sqrt{2}\sigma_y}\Big) - \operatorname{erf}\Big(\frac{y_1}{\sqrt{2}\sigma_y}\Big)\right). \end{gathered} \tag{34}$$

If the Gaussian is isotropic, then all axes are principal and expression (34) holds. When the Gaussian is not isotropic (say $\sigma_y < \sigma_x$) we may dilate the y direction by a factor σ_x/σ_y to make it isotropic, as shown in Fig. 10 (this transformation is also used in [8]). A dilation, like a projection, is a linear transformation. Therefore, it transforms parallel lines into parallel lines. If the eigenaxes of the dilation are not parallel to the sides of the rectangle, the rectangle is transformed not into another rectangle but into a parallelogram. However, if the rectangle is very elongated we can again argue as in subsubsection 3.1.2 and suppose that it will transform into almost another rectangle. In particular, we suppose that the dilation of the rectangle can be well approximated by a rectangle whose long axis is the dilated axis and whose width is the dilated width. Since the new Gaussian is isotropic, its axes may be rotated arbitrarily and still be principal axes. We rotate them so as to render them parallel to the sides of the dilated rectangle, as shown in Fig. 10, and then formula (34) can be applied.

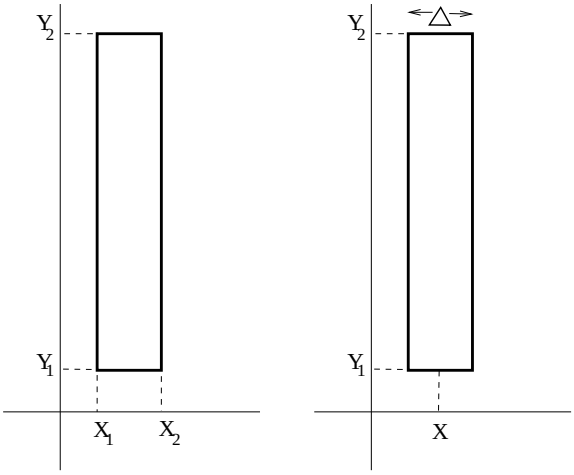

Fig. 9. The integral of a Gaussian over a rectangle of sides parallel to the principal axes of the Gaussian factorizes, yielding the result (34).

In order to adapt the result (34) to the approximation that we have described, we rewrite it as follows:

$$\begin{gathered} \frac{1}{2}\left(\operatorname{erf}\Big(\frac{x'+\Delta'/2}{\sqrt{2}\sigma_x}\Big) - \operatorname{erf}\Big(\frac{x'-\Delta'/2}{\sqrt{2}\sigma_x}\Big)\right) \cdot \\ \frac{1}{2}\left(\operatorname{erf}\Big(\frac{y_2'}{\sqrt{2}\sigma_y}\Big) - \operatorname{erf}\Big(\frac{y_1'}{\sqrt{2}\sigma_y}\Big)\right), \end{gathered} \tag{35}$$

where (x', y_1') and (x', y_2') are the coordinates of the end points of the dilated longitudinal axis of the tether in the new coordinates and Δ' is the width of the dilated rectangle.

Substitution of these four quantities into formula (35)

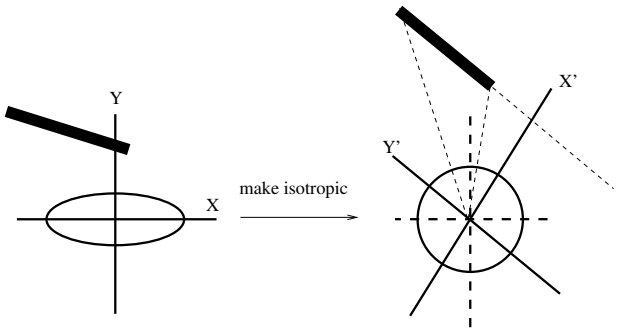

Fig. 10. The transformation shown allows the use of the simple formula (34) for the computation of the Gaussian probability above any thin rectangle.

yields:

$$\frac{1}{2}\left(\mathrm{erf}\Big(\frac{1}{\sqrt{2}}\frac{1}{\sigma_x\sigma_y}\frac{\sigma_y^2x_2(x_2-x_1)+\sigma_x^2y_2(y_2-y_1)}{\sqrt{\sigma_y^2(x_2-x_1)^2+\sigma_x^2(y_2-y_1)^2}}\Big)-\right.$$
$$\left.\mathrm{erf}\Big(\frac{1}{\sqrt{2}}\frac{1}{\sigma_x\sigma_y}\frac{\sigma_y^2x_1(x_2-x_1)+\sigma_x^2y_1(y_2-y_1)}{\sqrt{\sigma_y^2(x_2-x_1)^2+\sigma_x^2(y_2-y_1)^2}}\Big)\right).$$

$$\frac{1}{2}\left(\mathrm{erf}\Big(\frac{\sqrt{(x_2-x_1)^2+(y_2-y_1)^2}}{\sqrt{2}\sqrt{\sigma_y^2(x_2-x_1)^2+\sigma_x^2(y_2-y_1)^2}}\right.$$
$$\left.\Big(\frac{x_2y_1-x_1y_2}{\sqrt{(x_2-x_1)^2+(y_2-y_1)^2}}+\frac{\Delta}{2}\Big)\Big)-\right.$$

$$\mathrm{erf}\Big(\frac{\sqrt{(x_2-x_1)^2+(y_2-y_1)^2}}{\sqrt{2}\sqrt{\sigma_y^2(x_2-x_1)^2+\sigma_x^2(y_2-y_1)^2}}$$
$$\left.\Big(\frac{x_2y_1-x_1y_2}{\sqrt{(x_2-x_1)^2+(y_2-y_1)^2}}-\frac{\Delta}{2}\Big)\Big)\right). \quad (36)$$

The coordinates of the ends of the tether are good coordinates to derive the two preceding formulae, but are not as practical as the following five geometrical parameters: the b-plane coordinates (x and y) of the geometrical center of the rectangle, the rectangle length L and width Δ projected on the b-plane, and the orientation angle, Λ, of the longest rectangle axis with respect to the x eigenaxis of the covariance ellipsoid. In this way the coordinates of the four vertices of the rectangle in eq. (36) can be written as:

$$x_{1,2}=x\pm\frac{L}{2}\cos\Lambda;\qquad y_{1,2}=y\pm\frac{L}{2}\sin\Lambda, \quad (37)$$

leading to:

$$\frac{1}{4}\left\{\mathrm{erf}\left[\frac{D^2L/2+x\sigma_y^2\cos\Lambda+y\sigma_x^2\sin\Lambda}{\sqrt{2}D\sigma_x\sigma_y}\right]+\right.$$
$$\left.\mathrm{erf}\left[\frac{D^2L/2-x\sigma_y^2\cos\Lambda-y\sigma_x^2\sin\Lambda}{\sqrt{2}D\sigma_x\sigma_y}\right]\right\} \quad (38)$$
$$\left\{\mathrm{erf}\left[\frac{D/2+|y\cos\Lambda-x\sin\Lambda|}{\sqrt{2}D}\right]+\right.$$
$$\left.\mathrm{erf}\left[\frac{D/2-|y\cos\Lambda-x\sin\Lambda|}{\sqrt{2}D}\right]\right\},$$

where:

$$D\equiv\sqrt{\sigma_x^2\sin^2\Lambda+\sigma_y^2\cos^2\Lambda}. \quad (39)$$

4.3. The disk

The projection of a circle of radius r which makes an angle α with the encounter plane is an ellipse of semiaxes $r\cos\alpha$ and r. The Minkowski sum of this ellipse with a circle of radius R is not another ellipse, but it is enclosed by an ellipse of semiaxes $r\cos\alpha+R$ and $r\frac{r\cos\alpha+R}{r\cos\alpha}=\frac{r\cos\alpha+R}{\cos\alpha}$, as shown in Fig. 11.

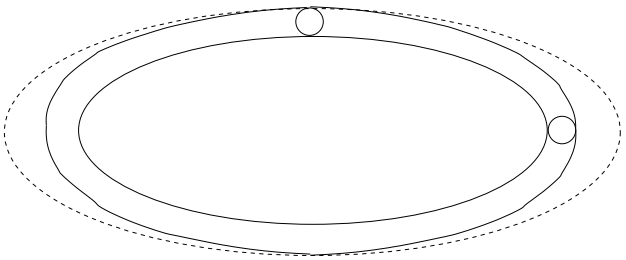

Fig. 11. The Minkowski sum of an ellipse and a circle is enclosed by the ellipse shown.

In order to find the probability enclosed by this ellipse we dilate along the direction of the shorter axis by a factor $1/\cos\alpha$, so that the ellipse becomes a circle. If the direction of the shorter axis is $\vec{w}$, then the sigmas of the Gaussian have to be multiplied by the factors $(\vec{w}\cdot\vec{i})/\cos\alpha$ and $(\vec{w}\cdot\vec{j})/\cos\alpha$, respectively. We are then in a position to apply any of a number of algorithms devised in the last decades in the field of spatial debris to compute the Gaussian probability caught by a circle [2, 3, 4, 5, 6, 7].

5. CONCLUSIONS

The formulae given in this article make it possible to improve the enveloping sphere or same area circle approximations for the computations of collision rates or probabilities when one of the objects is a circle, a rectangle or a very long rectangle or cylinder. This improvement is done without any additional

computational cost, since the formulae are all analytical except for the case of the collision probability of a rectangle, for which a very fast algorithm, available as an app, is provided.

The most direct application is to sails and tethers, which motivated this work, but other applications are possible. In general one may decompose a complex aircraft in various pieces, and separately compute the probability of collision for each. When one of the pieces is a solar panel then the formulae for the rectangle can be used. Of course this leaves the problem of mutual shadowing, but this would be a topic for future work.

6. ACKNOWLEDGMENTS

This work has been supported by the ESA Contract No. 4000119560/17/F/MOS ('Environmental aspects of passive de-orbiting devices'). This work has been supported by the Spanish Ministry of Economy and Competitiveness within the framework of the research project ESP2017-87271-P. We thank María de los Angeles Hernández Cifre and Hodei Urrutxua Cereijo for remarks and references.

7. REFERENCES

[1] Claudio Bombardelli and Javier Hernando-Ayuso, "Optimal impulsive collision avoidance in low earth orbit," *Journal of Guidance, Control, and Dynamics*, vol. 38, no. 2, pp. 217–225, 2015, doi: 10.2514/1.G000742.

[2] J. L. Foster and H. S. Estes., "A parametric analysis of orbital debris collision probability and maneuver rate for space vehicles," *NASA/JSC-25898*, 1992.

[3] Russell P. Patera, "General method for calculating satellite collision probability," *Journal of Guidance, Control, and Dynamics*, vol. 24, no. 4, pp. 716–722, 2001, doi: 10.2514/2.4771.

[4] F. Kenneth Chan, *Spacecraft Collision Probability*, American Institute of Aeronautics and Astronautics, 2008, ISBN-13: 978-1884989186, doi: 10.2514/4.989186.

[5] Salvatore Alfano, "A numerical implementation of spherical object collision probability," *Journal of the Astronautical Sciences*, vol. 53, no. 1, pp. 103–109, 2005.

[6] Romain Serra, Denis Arzelier, Mioara Joldes, Jean-Bernard Lasserre, Aude Rondepierre, and Bruno Salvy, "Fast and accurate computation of orbital collision probability for short-term encounters," *Journal of Guidance, Control and Dynamics*, vol. 39, no. 5, pp. 1009–1021, 2016, doi: 10.2514/1.G001353.

[7] Ricardo García-Pelayo and Javier Hernando-Ayuso, "Series for collision probability in short-encounter model," *Journal of Guidance, Control, and Dynamics*, vol. 39, no. 8, pp. 1908–1916, 2016, doi: 10.2514/1.G001754.

[8] Yuchen Xie and Ken Chan, "Collision probability for rectangular cross sections," in *2018 Space Flight Mechanics Meeting, AIAA SciTech Forum, (AIAA 2018-2231)*, 2018, doi: 10.2514/6.2018-2231.

[9] S. Alfano and D. Oltrogge, "Volumetric Encounter Analysis Enhancements," in *AAS/AIAA Astrodynamics Specialist Conference*, Vail, Colorado, USA, August 9-13 2015, AAS/AIAA, number AAS 15-581, pp. 1–37.

[10] Jer-Chyi Liou et al., "The new nasa orbital debris engineering model ordem2000," Tech. Rep., National Aeronautics and Space Administration, Johnson Space Center, 2002.

[11] S Flegel, J Gelhaus, C Wiedemann, P Vorsmann, M Oswald, S Stabroth, H Klinkrad, and H Krag, "The master-2009 space debris environment model," in *Fifth European Conference on Space Debris*, 2009, vol. 672.

[12] ISO 27852:2016, "Space systems – Estimation of orbit lifetime," Standard, International Organization for Standardization, Geneva, CH, July 2016.

[13] S. Alfano, "Accomodating Rectangular Objects in Probability Calculations," *AAS/AIAA Astrodynamics Specialist Conference and Exhibit, Paper No. AIAA 2004-5217*, 2004, doi: 10.2514/6.2004-5217.

[14] S. Alfano, "Method for determining maximum conjuction probability of rectangular-shaped objects," June 3 2008, US Patent 7,383,153 B2.

[15] Maruthi R. Akella and Kyle T. Alfriend, "Probability of collision between space objects," *Journal of Guidance, Control, and Dynamics*, vol. 23, no. 5, pp. 769–772, 2000, doi: 10.2514/2.4611.

[16] Vincent T. Coppola, "Including velocity uncertainty in the probability of collision between space objects," in *AAS/AIAA Spaceflight Mechanics Meeting*, 2012, AAS 12-247.

[17] Rolf Schneider, *Convex Bodies: The Brunn-Minkowski Theory*, Cambridge University Press, 2nd expanded edition edition, 2014, ISBN: 9780521352208.

[18] S. Alfano, "Eliminating Assumptions Regarding Satellite Conjunction Analysis," *AAS Journal of the Astronautical Sciences*, vol. 59, no. 4, pp. 676–705, 2012, doi: 10.1007/s40295-014-0002-4.

[19] F. Kenneth Chan, "Is the Probability of Collision of a Spacecraft Traversing Through the Earth's Debris Environment Described by a Poisson Distribution?," *27th*

Space Flight Mechanics Meeting, pp. 1–16, 2017, AAS 17-244.

[20] P. A. P. Moran, *An introduction to probability theory*, Clarendon Press, Oxford, 1968.

[21] H. Klinkrad, P. Wegener, C. Wiedemann, J. Bendisch, and H. Krag, *Space Debris: Models and Risk Analysis, Chapter 3: Modeling of the Current Space Debris Environment*, Springer, 2006, ISBN: 3-540-25448-X.

[22] Chuan Chih Hsiung, *A first course in differential geometry*, John Wiley & Sons, 1981, ISBN: 0-471-07953-7.

[23] Manuel Castellet and Irene Llerena, *Álgebra lineal y geometría*, Reverté, 1992, ISBN: 978-8429150094.

[24] AP Alpatov, VV Beletsky, VI Dranovskii, VS Khoroshilov, AV Pirozhenko, Hans Troger, and AE Zakrzhevskii, *Dynamics of Tethered Space Systems*, CRC Press, 2010, ISBN: 978-1-4398-3685-9.

[25] Alan Genz, "Numerical computation of rectangular bivariate and trivariate normal and t probabilities," *Statistics and Computing*, vol. 14, no. 3, pp. 251–260, 2004, doi: 10.1023/B:STCO.0000035304.20635.31.